Journal of
Marine Science and Engineering

MDPI

Article

The Impact of Model Resolution on the Southern Hemisphere in Community Climate System Model Version 4 Idealized Climate Simulations

Houraa Daher * and Ben P. Kirtman

Rosenstiel School for Marine, Atmospheric, and Earth Science, University of Miami, Miami, FL 33149, USA; bkirtman@earth.miami.edu
* Correspondence: hdaher@earth.miami.edu

Abstract: Model resolution plays a large role in accurately simulating the Southern Hemisphere circulation in both the ocean and atmosphere. Resolving the mesoscale field is important as it has been shown to have a significant impact on the large-scale climate in eddy-rich regions, which are regions of large CO_2 absorption. The presence of ocean and atmospheric mesoscale features can affect sea surface temperatures, the strength and location of storm tracks, and many other air-sea processes. Additionally, with an improvement in resolution, the eddy kinetic energy in the ocean can be expected to change considerably. The significance model resolution has on the Southern Hemisphere is examined using the Community Climate System Model, Version 4, eddy-parameterizing and eddy-resolving simulations. The CO_2 concentrations and ozone levels are specified independently to better understand how the mesoscale field responds to extreme changes in external forcing and the resulting climate impacts. Overall, in the eddy-parameterizing simulations, the ozone forcing is found to be more important than the changes in CO_2 concentrations. However, in the case of the eddy-resolving simulations, the CO_2 concentrations are found to be more dominant, especially in eddy-rich regions. These results demonstrate the need for an increase in model resolution for climate prediction.

Keywords: eddy-resolving; eddy-parameterizing; model resolution; CCSM4; CO_2 concentrations; ozone forcing

Citation: Daher, H.; Kirtman, B.P. The Impact of Model Resolution on the Southern Hemisphere in Community Climate System Model Version 4 Idealized Climate Simulations. *J. Mar. Sci. Eng.* **2023**, *11*, 2083. https://doi.org/10.3390/jmse11112083

Academic Editor: João Miguel Dias

Received: 15 September 2023
Revised: 26 October 2023
Accepted: 28 October 2023
Published: 31 October 2023

1. Introduction

Model resolution within global climate models has been shown to be of great importance when simulating the Southern Hemisphere climate. With an increase in model resolution, ocean and atmospheric mesoscale features are better resolved and play a large role in improving the accuracy of the large-scale climate within these models. These mesoscale features have a significant impact on the ocean circulation, atmosphere, and air-sea interactions [1–5], especially in eddy-rich regions like western boundary currents and their extensions [2,6–15]. In these regions, the mesoscale activity in the ocean drives the atmosphere with turbulent heat fluxes out of the ocean and into the atmospheric boundary layer [6]. Global climate models that use low-resolution model components are unable to capture these physical processes and, therefore, miss a large part of the climate picture. This study analyzes the importance of the mesoscale field in the Southern Hemisphere using the Community Climate System Model, Version 4 (CCSM4) eddy-parameterizing and eddy-resolving simulations.

The significance of both ocean and atmospheric model resolution in the Southern Hemisphere in CCSM4 has been demonstrated in previous studies. Bryan et al. [6] found that there is a positive correlation between sea surface temperature and surface wind stress when the ocean component is eddy-resolving. With an increase in model resolution, there is a stronger forcing of the atmosphere by the sea surface temperature variability in the extra-tropics that is found to be weak in the low-resolution model. Moreover, regions

of high mesoscale activity, like western boundary currents, are found to have a warmer sea surface temperature [16]. However, around Antarctica, the ocean warming response is found to be weaker with the presence of eddies in the model [17,18]. Additionally, a more accurate Agulhas current, retroflection, and leakage estimate is resolved using high-resolution eddy-resolving simulations [16,19–21]. Increasing the atmospheric model resolution component has important impacts as well. With an increase in resolution, the Southern Hemisphere westerly winds and wind stress are better resolved, resulting in an increase in the Southern Ocean mean flow meridional overturning circulation. This increase is partially compensated by the increase in ocean eddies, a significant result influencing the Atlantic Meridional Overturning Circulation [22].

Resolving the mesoscale features in these global climate models is not only important for understanding the physical processes but also for understanding the large-scale climate. Ocean eddies play a large role in the uptake of anthropogenic CO_2 [23], especially in the Southern Hemisphere, with 40% of the oceanic uptake of CO_2 occurring south of 40° S [24]. Additionally, resolving western boundary currents and their extensions has been shown to be as important, with these regions being hotspots of ocean warming, especially over the last few decades, where they have been warming at a rate of 3–4 times the global average [25–27]. Precipitation variability and drought are shown to be better predicted in the presence of mesoscale features in the ocean and atmosphere [28]. As mentioned previously, westerly winds in the Southern Hemisphere play a significant role in the global climate, and the increase observed is due to the increase in CO_2 concentrations and the depletion of stratospheric ozone. With anthropogenic climate change in the Southern Hemisphere being primarily driven by CO_2 concentrations and stratospheric ozone levels, the mesoscale field plays a significant role in changes to these atmospheric forces and, therefore, influences the Southern Hemisphere climate. This study examines how the mesoscale field responds to changes in CO_2 concentrations and ozone levels.

Bitz and Polvani [17] investigated the Antarctic climate response to stratospheric ozone depletion in CCSM4 and found that there is warming in the ocean down to 1000 m and reduced sea ice extent. They found that with the presence of ocean eddies, the warming is weaker, but the total loss of sea ice area is comparable between the eddy-resolving and eddy-parameterizing simulations. The weaker warming response in the presence of eddies is a process known as eddy compensation, in which the mesoscale eddies oppose the wind-driven upwelling that is often seen with increased CO_2 concentrations and stratospheric ozone depletion and, therefore, prevent long-term warming [29]. Using observations and climate models, Swart et al. [30] find that the warming and freshening of the Southern Ocean are driven primarily by an increase in anthropogenic greenhouse gases and that the effect of stratospheric ozone depletion is secondary. Using a unique coupled climate model with enhanced ocean resolution, Ivanciu et al. [31] investigate the impact of increased greenhouse gases and ozone recovery on the Southern Hemisphere and find the westerly winds weaken and shift equatorward due to ozone recovery, resulting in a decrease in transport of the Antarctic Circumpolar Current (ACC) and in Agulhas leakage. They also find warming in the upper ocean is associated with increased greenhouse gases that overwhelm the ozone recovery signal.

The impact of model resolution on the Southern Hemisphere in CCSM4 is studied using eddy-parameterizing and eddy-resolving simulations. Past CO_2 concentrations and stratospheric ozone levels are specified independently to simulate idealized climate states to investigate what role the presence of ocean and atmospheric eddies plays in the Southern Hemisphere's large-scale ocean circulation and air–sea interactions. This paper compares the individual responses of low-resolution eddy-parameterizing simulations against high-resolution eddy-resolving simulations when the external forcing is idealized to include an increase in CO_2 concentrations and stratospheric ozone levels from the mid-twentieth century. The results presented here are not intended to be interpreted as projections or predictions. The intent is to diagnose how the response to large changes in CO_2 and ozone concentrations differ in low-resolution eddy parameterized vs. high-resolution eddy-permitting global coupled simulations.

2. Materials and Methods

This study analyzes model output from NCAR's CCSM4 coupled-climate model [32]. The ocean and atmosphere models used in CCSM4 are the Parallel Ocean Program, Version 2 (POP2), and Community Atmosphere Model, Version 4 (CAM4), respectively. POP2 has 60 vertical layers with a 10 m layer thickness in the first 100 m and slowly increasing to 250 m at 6000 m depth. CAM4 has 26 vertical layers in the atmosphere. The stratospheric and tropospheric ozone are calculated semi-offline using the interactive chemistry in CAM-Chem, the chemistry version of CAM [33–37]. The land and ice models used in CCSM4 are the Community Land Model, Version 4 (CLM4), and the Los Alamos National Laboratory sea-ice model, Community Ice CodE, Version 4 (CICE4). However, only variables from the ocean and atmosphere models are considered in this study. All model components communicate using the CCSM coupler, CPL7 [38]. POP2 uses the Gent–McWilliams isopycnal transport parameterization [39], near-surface eddy flux parameterization [40], and submesoscale mixing parameterization [41]. CAM4 uses the Lin-Rood finite volume discretization [42]. More specific information on the parameterizations, schemes, and coefficients used in CCSM4 can be found in Kirtman et al. [16], Gent et al. [32], and Yeager and Danabasoglu [43], where they are discussed in great detail.

Model output from six simulations is used, a combination of two model resolutions and three idealized experiments (Table 1). The eddy-parameterizing simulations are low-resolution, with 1° in the ocean and atmosphere, and the eddy-resolving simulations are high-resolution, with 1/10° in the ocean and 1/2° in the atmosphere. The first idealized experiment (LRC08 for the low-resolution simulation and HRC08 for the high-resolution simulation) is the control experiment with the CO_2 forcing kept constant at year 2000 levels (379 ppm, Figure 1a, red line). The ozone levels are also kept constant at year 2000 levels, a time representative of depleted ozone (Figure 1b, red line). There are 100 years of data available for LRC08, and 70 years of data are available for HRC08. LRC08 and HRC08 are used as the control experiments, as the CO_2 concentrations and ozone levels are both kept constant, unlike the other two experiments. Any differences between the control experiment and these other experiments can be attributed to changes in the forcing parameters. The second idealized experiment (LRC07 and HRC07) is the 20th-century climate change simulation with corresponding CO_2 levels applied [16] (Figure 1a, blue line). The ozone levels in this experiment are also kept constant at year 2000 levels. Like LRC08 and HRC08, 100 years of data are available for LRC07 (1910–2010), and 70 years of data are available for HRC07 (1940–2009). The LRC07 and HRC07 simulations are interpreted as idealized experiments examining how changes in CO_2 concentrations affect the Southern Hemisphere climate with fixed (depleted) ozone concentrations. This approach is useful in terms of separating the effects of CO_2 changes from ozone changes. The last idealized experiment (LRC20 and HRC20) uses the constant year 2000 CO_2 forcing (Figure 1a, red line) like the control experiment but sets the ozone to the year 1955 levels, a time representative of a healthier ozone (Figure 1b, blue line). LRC20 has 100 years of data; however, HRC20 only has 20 years of data available as the mean climatic effects become clear in a relatively short period of time. Month-mean outputs are considered in this study.

Table 1. List of the six CCSM4 experiments used in this study. Low resolution is equal to 1° in both the atmosphere and ocean, and high resolution is 1/2° in the atmosphere and 1/10° in the ocean.

Name	Resolution	CO_2 Concentrations	Ozone	Years
LRC07	Low	Historical CO_2	Year 2000 O_3	100 years
LRC08	Low	Year 2000 CO_2	Year 2000 O_3	100 years
LRC20	Low	Year 2000 CO_2	Year 1955 O_3	100 years
HRC07	High	Historical CO_2	Year 2000 O_3	70 years
HRC08	High	Year 2000 CO_2	Year 2000 O_3	70 years
HRC20	High	Year 2000 CO_2	Year 1955 O_3	20 years

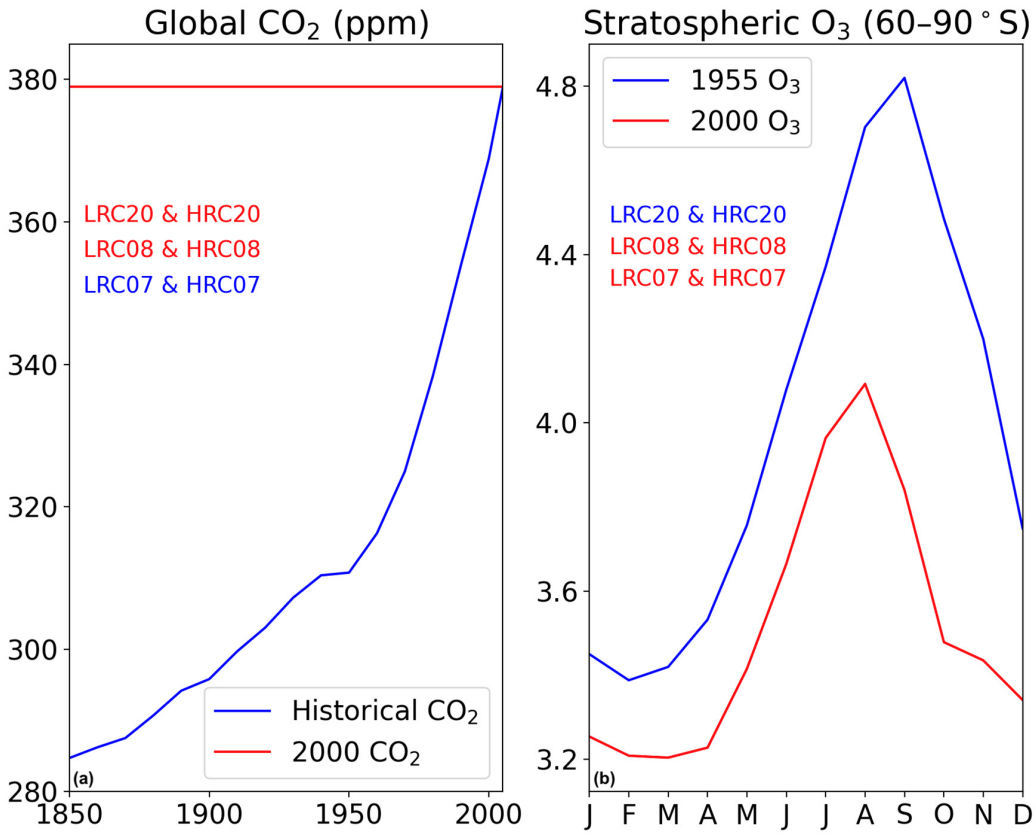

Figure 1. The CO_2 concentrations and O_3 forcing were used in the CCSM4 simulations. (**a**) The year 2000 CO_2 levels are shown in red (LRC08 and HRC08 and LRC20 and HRC20), and historical ozone is shown in blue (LRC07 and HRC07); (**b**) the 1955 ozone levels are shown in blue (LRC20 and HRC20), and the 2000 ozone levels are shown in red (LRC07 and HRC07 and LRC08 and HRC08).

The first objective in comparing these simulations is to identify any differences between the eddy-parameterizing and eddy-resolving experiments, with specific attention to the Southern Hemisphere climate. The second objective is to examine what role the difference in model resolution plays in the idealized experiments and how the presence of a more robustly represented mesoscale field affects the response to changes in atmospheric forcing, specifically changes in atmospheric CO_2 and ozone levels. To examine the Southern Hemisphere response to changes in CO_2 (while holding the ozone levels constant), a difference between the time-averaged mean of the high concentrations warming experiment (LRC08 and HRC08) and the time-averaged mean of the low concentrations cooling experiment (LRC07 and HRC07) is taken. These differences are referred to as LRC_{CO_2} and HRC_{CO_2}. The same can be conducted to determine the Southern Hemisphere response to changes in the ozone (while holding the CO_2 levels constant) by taking a difference between the time-averaged mean of the healthier ozone experiment (LRC20 and HRC20) and the time-averaged mean of the depleted ozone experiment (LRC08 and HRC08). These differences are referred to as LRC_{O_3} and HRC_{O_3}. Because the radiative forcing associated with the changes in CO_2 and O_3 is different, the results are normalized by the global mean temperature change to put them on equal footing. LRC_{CO_2}, HRC_{CO_2}, LRC_{O_3}, and HRC_{O_3} are divided by the difference in the global mean surface air temperature (2 m temperature, TS) for their respective experiments. The normalized quantities are interpreted as the response per degree of global mean temperature change. This normalization allows for quantitative comparisons of the CO_2 vs. O_3 response. This approach of normalizing by global mean temperature is seen in previous climate studies [44–50]. Lastly, to find the net change and whether the CO_2 or ozone forcing is more dominant, a sum of the CO_2 and ozone differences is taken.

For the CO_2 forcing, change per degree of warming:

$$LRC_{CO_2} = \frac{LRC08 - LRC07}{|\overline{TS_{LRC08}} - \overline{TS_{LRC07}}|} \;\&\; HRC_{CO_2} \frac{HRC08 - HRC07}{|\overline{TS_{HRC08}} - \overline{TS_{HRC07}}|}$$

For the O_3 forcing, changer per degree of cooling:

$$LRC_{O_3} = \frac{LRC20 - LRC08}{|\overline{TS_{LRC20}} - \overline{TS_{LRC08}}|} \;\&\; HRC_{O_3} = \frac{HRC20 - HRC08}{|\overline{TS_{HRC20}} - \overline{TS_{HRC08}}|}$$

The sum of these normalized maps is then used to obtain the net change:

$$LRC_{Total} = LRC_{CO_2} + LRC_{O_3} \;\&\; HRC_{Total} = HRC_{CO_2} + HRC_{O_3}$$

3. Results

The following figures (Figures 2–9) show the mean differences between the ocean eddy-parameterizing and eddy-resolving simulations as well as the differences between the increased CO_2 concentrations and ozone of the past. The first row shows the results from the eddy-parameterizing experiments (LRC), and the second row shows the results from the eddy-resolving experiments (HRC). The first, second, and third columns show results from LRC_{CO_2} and HRC_{CO_2}, LRC_{O_3} and HRC_{O_3}, and LRC_{Total} and HRC_{Total}, respectively.

3.1. Zonal Mean Atmospheric Temperature

The next two figures (Figures 2 and 3) examine the response to the zonal mean atmospheric temperature and the zonal mean zonal wind. The zonal mean temperature throughout the atmosphere is calculated at each latitude (Figure 2). In LRC_{CO_2} (Figure 2a), there is warming seen throughout the Southern Hemisphere except in the lower stratosphere poleward of 50° S, where the ozone is depleted and cooling in the lower stratosphere is observed. The strongest changes in temperature are seen at 100 mb, with an increase (decrease) in over two degrees equatorward (poleward) of 50° S. The ozone layer is in the upper 100 mb and shows how the increase in CO_2 concentration strongly influences the zonal mean atmospheric temperature. The high-resolution equivalent, HRC_{CO_2} (Figure 2d), shows a similar response as LRC_{CO_2} with cooling in the lower stratosphere, but this cooling extends beyond the high latitudes to the equator in the top 100 mb. There is also a slight cooling seen at the surface in the high latitudes that is not present in the low-resolution simulation. Overall, the average change in the Southern Hemisphere zonal mean atmospheric temperature is 0.26 °C/°C in LRC_{CO_2} and −0.21 °C/°C in HRC_{CO_2}, showcasing the difference the resolution can have on the changes observed overall.

The LRC_{O_3} (Figure 2b) map shows an opposite and more intense pattern to LRC_{CO_2}, with a stronger warming seen in the lower stratosphere poleward of 50° S. Warming of much greater than two degrees is seen when the ozone levels are representative of the past. A healthy ozone layer above Antarctica means most of the incoming solar radiation will be absorbed by the lower stratosphere at the high latitudes, and there will be less warming throughout the atmosphere. HRC_{O_3} (Figure 2e) also shows warming in the lower stratosphere at high latitudes, but it is not as strong as in LRC_{O_3}. However, there is a strong cooling of more than two degrees seen equatorward of 55° S between 200 and 600 mb that is not present in LRC_{O_3}. The average change in the ozone scenario is different from the CO_2 scenario in that both the low-resolution and high-resolution scenarios show a decrease in the zonal mean atmospheric temperature but of different magnitudes. The change in LRC_{O_3} is −0.17 °C/°C, and the change in HRC_{O_3} is −0.59 °C/°C, over three times the ozone signal in the low-resolution simulation.

The intense warming seen in LRC_{O_3} (Figure 2b) is also present in LRC_{Total} (Figure 2c), suggesting that the ozone forcing dominates in the lower stratosphere. The rest of the atmosphere has little to no temperature change, with the two responses largely canceling each other out. The overall net change seen in HRC_{Total} (Figure 2f) is slightly different

from LRC_{Total} as there is only a small region of the lower stratosphere warming at the high latitudes and cooling associated everywhere else. The upper 100 mb looks to be controlled by the increase in CO_2 concentrations, whereas the rest of the Southern Hemisphere shows a response similar to the 1955 ozone simulation. Overall, the biggest change observed with an increase in atmospheric resolution is the magnitude of change (with a change of nearly zero, 0.09 °C/°C, in LRC_{Total} compared to a change of −0.80 °C/°C in HRC_{Total}). However, the pattern between the two remains consistent, with the ozone forcing being more important than the CO_2 concentrations, particularly for the eddy-resolving simulations.

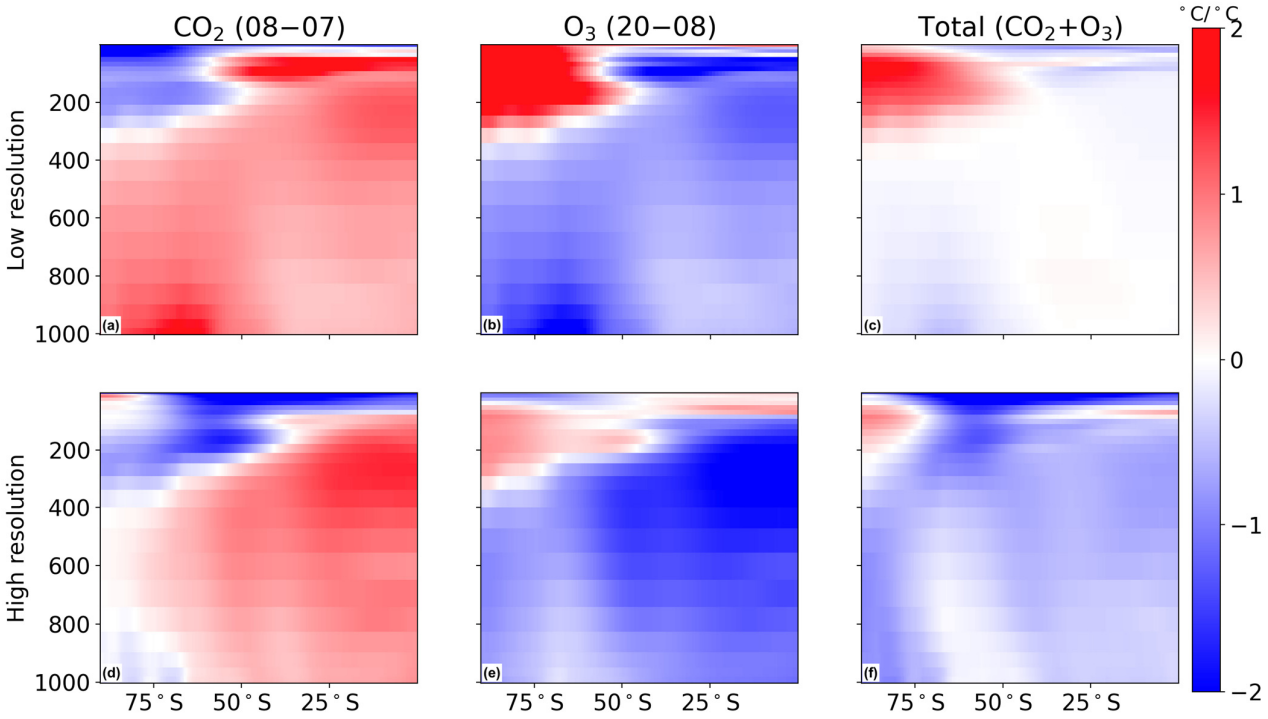

Figure 2. The zonal mean Southern Hemisphere atmospheric temperature in the eddy-parameterizing simulations (**a**–**c**) and eddy-resolving simulations (**d**–**f**) for the increased CO_2 concentrations (**a**,**d**), past ozone from 1955 (**b**,**e**), and net change (**c**,**f**). The atmospheric height in millibars is shown on the y-axis, and the latitude is shown on the x-axis.

3.2. Zonal Mean Zonal Wind

The same calculation for the atmospheric temperature is performed for the zonal wind (Figure 3), and the patterns seen in the LRC simulations (Figure 3a–c) are all relatively weak compared to the HRC simulations (Figure 3d–f). In LRC_{CO_2}, there is an increase in the zonal mean zonal wind found in the upper 200 mb at the mid-latitudes and a slight increase in the westerlies and towards the equator. This is in agreement with previous studies that show an increase in Southern Hemisphere westerlies with an increase in CO_2 concentrations. There is a decrease in zonal wind seen at the trade wind latitudes. The pattern seen in HRC_{CO_2} (Figure 3d) is similar to LRC_{CO_2} but much stronger. There is a strong increase in the westerlies and upper troposphere equatorward of 55° S. This strong increase in the Southern Hemisphere westerlies plays a significant role in the large-scale climate picture, as mentioned previously, and demonstrates the need for higher-resolution coupled-climate models moving forward to improve future climate prediction, especially as CO_2 concentrations continue to increase. The average change in LRC_{CO_2} is 0.48 ms^{-1}/°C, whereas in HRC_{CO_2}, it nearly doubles and is 0.90 ms^{-1}/°C, likely due to the strong increase in the westerlies observed.

Similar to what was observed with the zonal mean temperature (Figure 2), the opposite pattern to LRC_{CO_2} is shown for the LRC_{O_3} (Figure 3b) simulation, with a slight decrease

in the westerlies and a stronger decrease observed in the upper 200 mb. However, for HRC_{O_3} (Figure 3e), the signal is much more amplified throughout the atmosphere, and there is a strong weakening of the westerly jet and upper troposphere. The average change between the two does not differ much between the two, with -0.74 ms^{-1}/°C in LRC_{O_3} and -0.68 ms^{-1}/°C in HRC_{O_3}.

LRC_{Total} (Figure 3c) shows very little change, with the exception of the upper 100 mb resembling the LRC_{O_3} simulation. HRC_{Total} (Figure 3f) shows a different response, showing that at the equatorward of 50° S, the increase in CO_2 concentrations plays a larger role, and at the poleward of 50° S, the ozone is more important. It is also clear in the low-resolution simulations that there is no poleward or equatorward shift of the westerlies, whereas the high-resolution simulations show an equatorward shift and weakening of the westerly jet. Both simulations have a similar magnitude of change but with the opposite sign, with -0.26 ms^{-1}/°C in LRC_{Total} and 0.23 ms^{-1}/°C in HRC_{Total}.

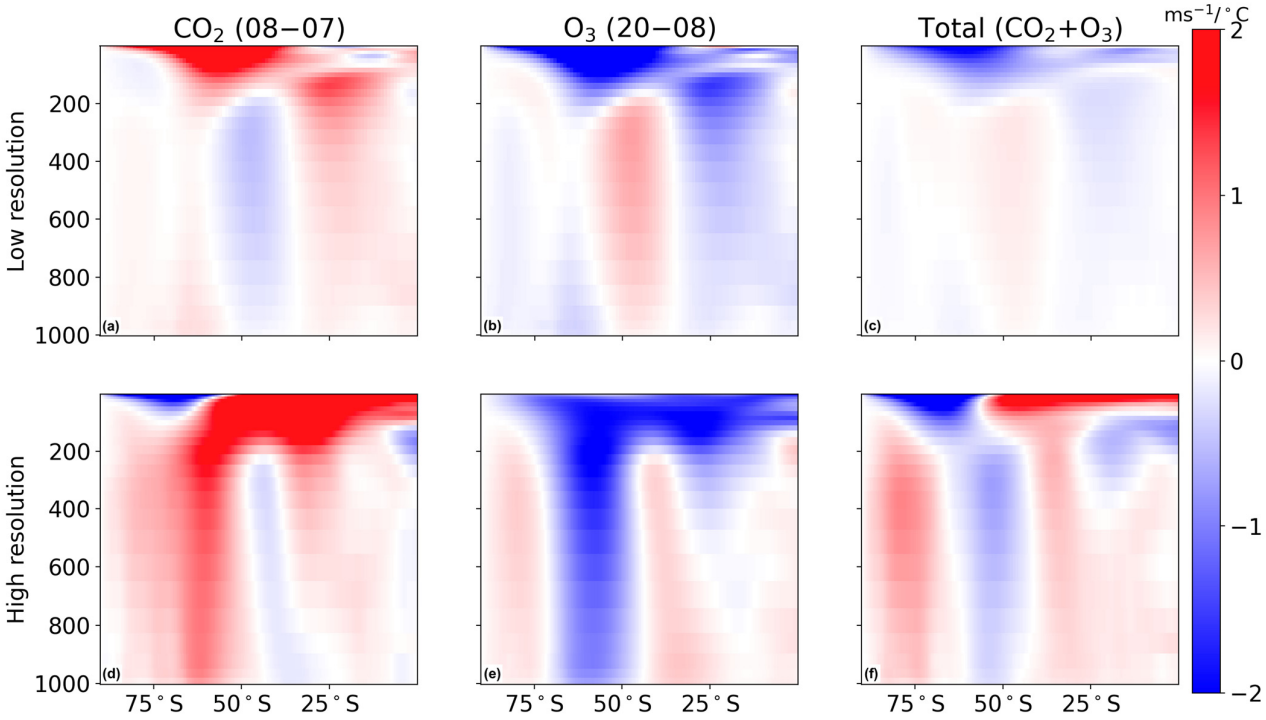

Figure 3. The Southern Hemisphere zonal mean zonal wind in the eddy-parameterizing simulations (**a**–**c**) and eddy-resolving simulations (**d**–**f**) for the increased CO_2 concentrations (**a**,**d**), past ozone from 1955 (**b**,**e**), and net change (**c**,**f**). The atmospheric height in millibars is shown on the y-axis, and the latitude is shown on the x-axis.

While there are slight differences in the methods of showing the results, the zonal mean temperature and zonal mean zonal wind in this study (Figures 2 and 3) are compared with those in Figure 1 from Polvani et al. [51]. They used an atmospheric model (CAM3, 2.8° × 2.8° horizontal resolution), and the results were found to be in good agreement. With an increase in concentrations, Polvani et al. [51] find a decrease in the temperature at the high latitudes in the lower stratosphere that extends to the equator in the upper 100 mb and an increase in temperature everywhere else in the Southern Hemisphere, a result consistent with HRC_{CO_2} (Figure 2d). In their ozone recovery simulation, they found intense warming in the lower stratosphere more closely resembling LRC_{O_3} (Figure 2b) compared to HRC_{O_3}. The net change results from Polvani et al. [51] continue to show an increase in this region at the high latitudes with cooling at the very top of the atmosphere, features that are both seen in LRC_{Total} and HRC_{Total} (Figure 2c,f). The results from the zonal mean zonal wind calculation in Polvani et al. [51] agree with the HRC simulations

shown previously (Figure 2d–f). The result of increasing concentrations is an increase and poleward shift of the westerlies that can also be seen in HRC_{CO_2} (Figure 3d). The more intense weakening and equatorward shift seen with the ozone recovery is found in HRC_{O_3} (Figure 3e). The overall trend is an equatorward shift and weakening of the westerlies, especially in the upper 200 mb, consistent with what is found in HRC_{Total} (Figure 3f).

3.3. Sea Surface Temperature

Next, the results from the sea surface temperature (SST) are analyzed (Figure 4). Beginning with LRC_{CO_2} (Figure 4a), there is roughly one-degree warming everywhere except in the Southern Ocean, where there is intense warming observed in the Southern Ocean of nearly three degrees. With the increase in CO_2 concentrations, there is warming everywhere in the Southern Hemisphere oceans, except for one small region in the South Pacific. The average change in the Southern Hemisphere sea surface temperatures for LRC_{CO_2} is 0.58 °C/°C. In the eddy-resolving case, HRC_{CO_2} (Figure 4d), the results do not differ much from the eddy-parameterizing case, with warming observed nearly everywhere, including the Southern Ocean, where the presence of eddies shows a strong increase in SSTs. This warming is seen in eddy-rich regions like the Agulhas retroflection and the Brazil–Malvinas Confluence Zone. However, unlike LRC_{CO_2}, there is cooling seen in the high latitudes near Antarctica (see also Bilgen and Kirtman [18]), weakening the average change observed, which is found to be 0.32 °C/°C.

LRC_{O_3} (Figure 4b) shows an opposite but similar pattern to LRC_{CO_2}, with cooling seen throughout all the oceans and warming in the same small region in the South Pacific. The HRC_{O_3} simulation (Figure 4e) also shows cooling nearly everywhere except around Antarctica, where a slight warming is observed. In contrast with the low-resolution simulation, however, the cooling seen over the Southern Ocean and the ACC is much weaker. Additionally, the strong eddy response observed in HRC_{CO_2} is not present with the changed ozone. As mentioned previously, the weak cooling response observed in HRC_{O_3} is likely due to eddy compensation, with the presence of eddies dampening the response in SSTs over the Southern Ocean as changes in atmospheric forcing are experienced [29]. The increase in model resolution also influences the weak cooling and increase in eddy compensation observed here, as was discussed in Gent [22]. The eddy compensation does not weaken the average change observed by much as the magnitude between the two simulations is similar with −0.65 °C/°C and −0.56 °C/°C in LRC_{O_3} and HRC_{O_3}, respectively.

Overall, the net change shown in LRC_{Total} (Figure 4c) is small, suggesting that the increased CO_2 concentrations and 1955 ozone levels largely cancel each other out with respect to SST, with only −0.07 °C/°C observed throughout the Southern Hemisphere. In the Indian and Pacific Oceans, there is a slight warming observed, demonstrating that the CO_2 forcing is stronger here. In contrast, there is cooling everywhere else, showing that the ozone signal is larger, especially near Antarctica, which, with 1955 ozone levels, is no longer as exposed to solar radiation. The total net change seen in HRC_{Total} (Figure 4f) is larger than LRC_{Total}, with −0.24 °C/°C observed, and is mostly dominated by the ozone forcing and cooling seen in most of the Southern Hemisphere. The eddy-rich regions identified previously undergo warming and cooling, highlighting the importance of both CO_2 and ozone. However, the increase in CO_2 concentrations and heat trapped within the eddies plays a larger role in these regions, and these eddies weaken the SST gradient.

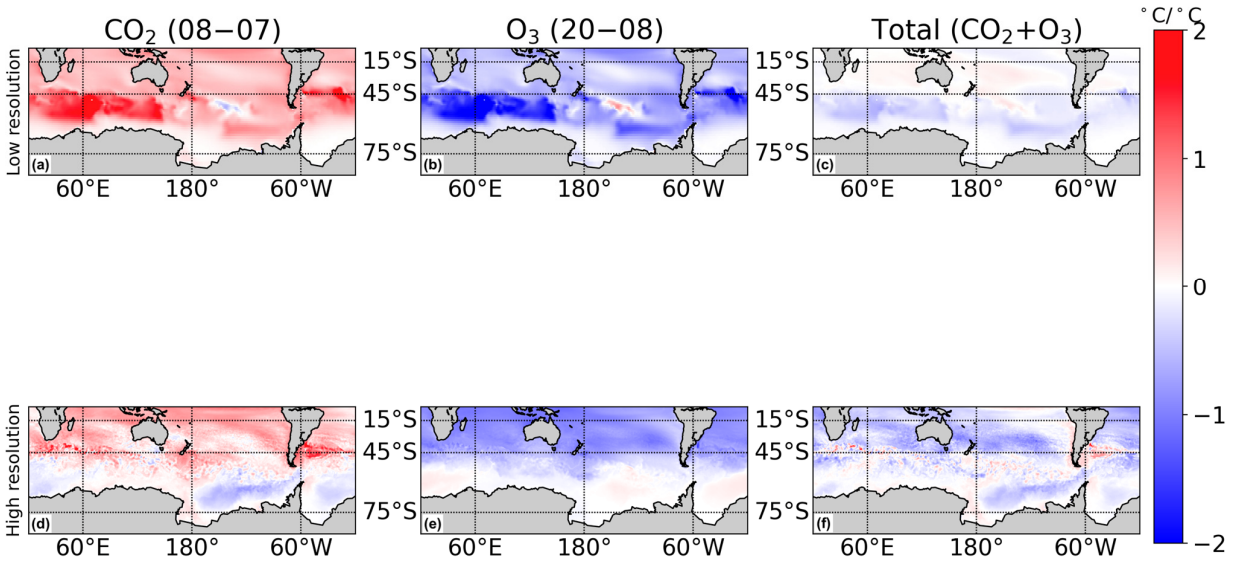

Figure 4. The Southern Hemisphere sea surface temperature in the eddy-parameterizing simulations (**a**–**c**) and eddy-resolving simulations (**d**–**f**) for the increased CO_2 concentrations (**a**,**d**), past ozone from 1955 (**b**,**e**), and net change (**c**,**f**).

3.4. Sea Surface Height

For the sea surface height (SSH), with an increase in CO_2 concentrations in LRC_{CO_2} (Figure 5a), there is an increase in SSH seen everywhere except south of the ACC and most of the South Atlantic. The pattern seen in HRC_{CO_2} (Figure 5d) closely resembles the pattern seen in the LRC equivalent, with the exception of the eddies. In HRC_{CO_2}, the magnitude of change is comparable to LRC_{CO_2}, and the eddies in the Agulhas retroflection and Brazil–Malvinas Confluence Zone show an increase in SSH. The average change in both simulations is small, with -0.015 m/°C found in LRC_{CO_2} and -0.034 m/°C in HRC_{CO_2}.

For LRC_{O_3} (Figure 5b), an opposite pattern is seen compared to LRC_{CO_2}, with an increase in sea level expected south of the ACC and South Atlantic with 1955 ozone levels. The average change found is 0.019 m/°C. Once again, the pattern in the high-resolution simulation of HRC_{O_3} (Figure 5e) is similar to the low-resolution simulation. However, the magnitude of change is much smaller than what is seen in both LRC_{O_3} and HRC_{CO_2}, 0.007 m/°C. Moreover, the eddies are not associated with much change, similar to what was shown in the HRC_{O_3} SST map (Figure 4e).

The net change is once again weak, 0.004 m/°C, in LRC_{Total} (Figure 5c), but the pattern resembles that of the LRC_{O_3} case, especially poleward of 45° S, suggesting that the ozone forcing is slightly more important in the low-resolution eddy-parameterizing model. However, the SSH pattern seen in HRC_{Total} (Figure 5f) closely resembles HRC_{CO_2}, demonstrating that the increased CO_2 concentrations dominate in the high-resolution eddy-resolving model. The average change in HRC_{Total} is -0.024 m/°C, very similar to what was observed in HRC_{CO_2}.

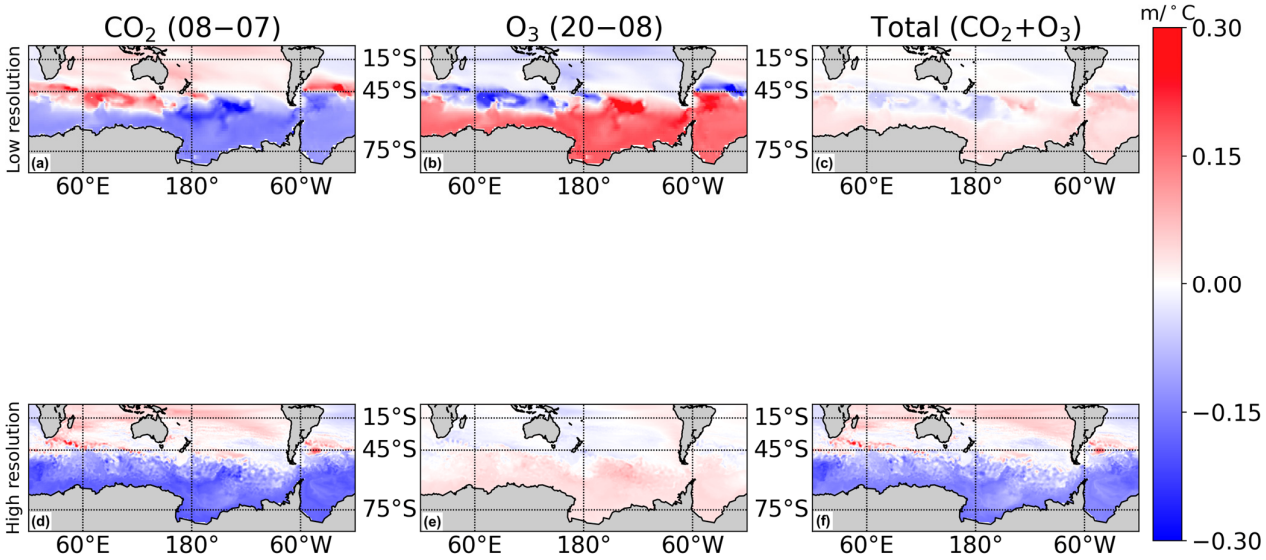

Figure 5. The Southern Hemisphere sea surface height in the eddy-parameterizing simulations (**a**–**c**) and eddy-resolving simulations (**d**–**f**) for the increased CO_2 concentrations (**a**,**d**), past ozone from 1955 (**b**,**e**), and net change (**c**,**f**).

3.5. Eddy Kinetic Energy

The eddy kinetic energy (EKE $= 0.5(u'^2 + v'^2)$, $u' = u - \overline{u}$, $v' = v - \overline{v}$) is calculated for each simulation. For LRC_{CO_2} (Figure 6a), there is a weak EKE response since it is not an eddy-resolving model. There is a small signal in the equatorial region, with increases and decreases in EKE observed. In the eddy-resolving simulations, the presence of eddies is evident as the changes are seen throughout the Southern Hemisphere in HRC_{CO_2} (Figure 6d). A change of -0.12 cm^{2}s^{-2}/°C is found in the LRC_{CO_2} eddy kinetic energy. In HRC_{CO_2} (Figure 6d), there is an increase in EKE in the ACC, the open Pacific Ocean, along the coast of Africa, through the Mozambique Channel, and the Agulhas retroflection associated with an increase in CO_2 concentrations. There is a decrease in EKE in the equatorial region, near the East Australian Current and Brazil–Malvinas Confluence Zone, and parts of the Agulhas retroflection. The average change in HRC_{CO_2}, -0.59 cm^{2}s^{-2}/°C, is roughly five times the change observed in LRC_{CO_2}.

LRC_{O_3} (Figure 6b) shows a similar but oppositely weak response in EKE as LRC_{CO_2}, with the largest signal observed in the equatorial regions. Again, the high-resolution simulation of HRC_{O_3} (Figure 6e) shows a larger EKE response. However, compared to the HRC_{CO_2} simulation, the HRC_{O_3} simulation is less active, and values are not as large. There is an increase in EKE in the equatorial Pacific and the subtropical Pacific and Indian Oceans, and a decrease seen in the majority of the ACC. Despite the significant changes observed in these eddy-rich regions, the corresponding SST and SSH maps (Figures 4e and 5e) have a weak signal as a response to the eddy compensation mechanism described previously and in previous studies [31], which dampens the signal observed. Mean changes of 0.67 cm^{2}s^{-2}/°C and -0.06 cm^{2}s^{-2}/°C are found in LRC_{O_3} and HRC_{O_3}, respectively.

The pattern from LRC_{Total} (Figure 6c), although small, more closely resembles the pattern from LRC_{O_3}, with a similar change in magnitude of 0.55 cm^{2}s^{-2}/°C. This suggests that the ozone forcing is slightly stronger than the increased CO_2 forcing in the eddy-parameterized model, agreeing with the result of the previous SSH figure (Figure 5), which shows a slightly stronger response to the 1955 ozone levels. In the high-resolution simulations, between the two forces, the increase in CO_2 is more dominant, as the average change is -0.65 cm^{2}s^{-2}/°C, similar to what was observed in HRC_{CO_2}. The pattern seen in HRC_{Total} (Figure 6f) is strikingly similar to HRC_{CO_2}. The strong changes in EKE observed in response to increased CO_2 concentrations could be explained by eddy saturation, especially over the Southern Ocean, where this phenomenon has been known to take place [52–54].

Eddy saturation occurs when there is an intensification of the winds and an increase in the wind stress (i.e., due to the increase in CO_2 concentrations), and the increased momentum is then transferred to the ocean mesoscale, therefore creating a more energetic eddy field as a result.

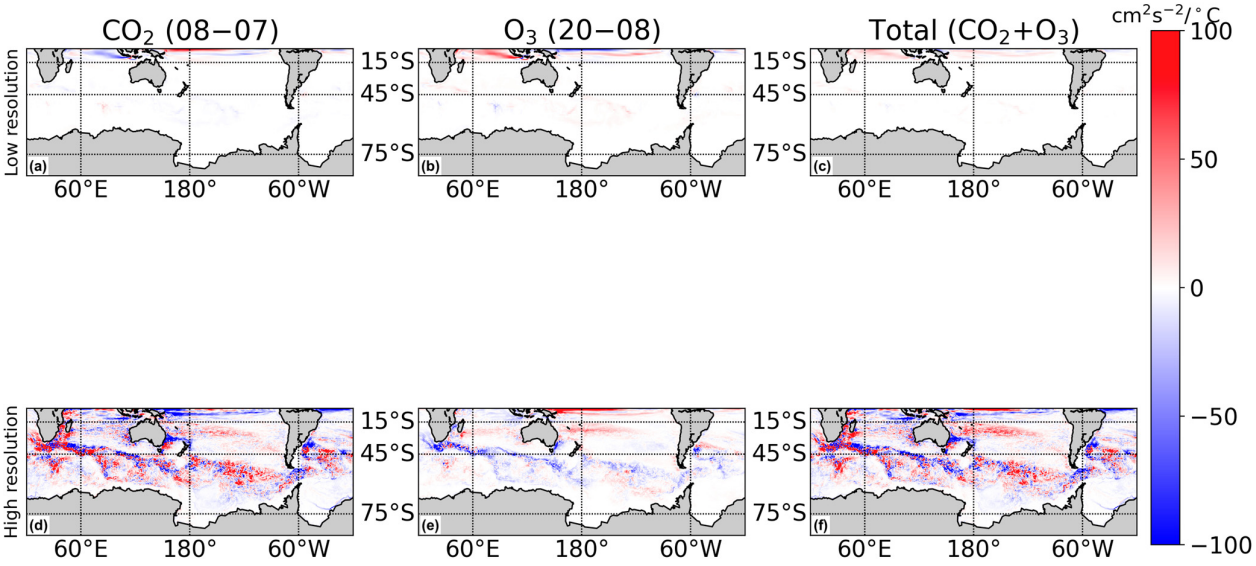

Figure 6. The Southern Hemisphere eddy kinetic energy in the eddy-parameterizing simulations (**a**–**c**) and eddy-resolving simulations (**d**–**f**) for the increased CO_2 concentrations (**a**,**d**), past ozone from 1955 (**b**,**e**), and net change (**c**,**f**).

3.6. Zonal Mean Ocean Temperature

The zonal mean ocean temperature is calculated at each latitude throughout the Southern Hemisphere (Figure 7). With the increase in CO_2 concentrations in LRC_{CO_2} (Figure 7a), there is an increase in the ocean temperature observed throughout the entire vertical structure of the ocean, with the exception of one small region of cooling found near 35° S at 1000 m. The greatest warming in this scenario is found poleward at 40° S with strong increases at the surface and 2000 m. However, the HRC case shows a very different response than the LRC case, with an overall weaker, less uniform response. The average change is found to be 0.44 °C/°C. In HRC_{CO_2} (Figure 7d), the strongest increase in temperature is found at the surface equatorward of 50° S. In addition to the surface, there are strong increases in temperature found down to the intermediate depths near Antarctica, 50° S, and near the equator. These locations coincide with areas of increased EKE (Figure 6d). The increased temperature in these regions is likely influenced by the presence of eddies from the ACC, western boundary currents, and equatorial currents. The weaker response to the zonal mean ocean temperature in HRC_{CO_2} is 0.08 °C/°C.

Consistent with previous results from the LRC simulations, a similar but opposite pattern is seen in LRC_{O_3} (Figure 7b). Almost everywhere, it cools, except for the location of cooling observed in LRC_{CO_2}, where there is warming. The mean change is found to be similar in magnitude but opposite in sign as well, with −0.53 °C/°C observed. In HRC_{O_3} (Figure 7e), there is cooling observed nearly everywhere, with the strongest decrease in temperature found in the upper 1000 m and little change seen at deeper depths. The decrease in temperature found at 50° S is located at the same latitude where there is a strong zonal mean decrease in EKE (Figure 6e). Like HRC_{CO_2}, a weaker magnitude is observed in the high resolution, with a change of only −0.18 °C/°C.

The overall change in LRC_{Total} (Figure 7c) shows that ozone is the stronger of the two forced responses. In the LRC simulations (Figure 7a–c), the impact of increased CO_2 concentrations and past ozone is seen at depth, suggesting a strong mixing component in the eddy-parameterizing simulations as the changes are nearly uniform throughout the

water column, especially towards Antarctica. However, HRC_{Total} (Figure 7f) shows the ozone signal is only stronger in the upper 500 m equatorward of 50° S and that the increase in CO_2 concentrations plays a larger role elsewhere, especially at the intermediate depths in eddy-rich regions. The HRC maps also show that the decrease (increase) in SST observed near Antarctica (Figure 4d,e) with the increased CO_2 concentrations (1955 ozone levels) occurs only at the surface in the upper 200 m, and there is an increase (decrease) found at the depth directly below. The mean differences in the Southern Hemisphere zonal mean ocean temperature are found to be similar in the low-resolution and high-resolution simulations, with changes of −0.09 °C/°C and −0.10 °C/°C found in LRC_{Total} and HRC_{Total}.

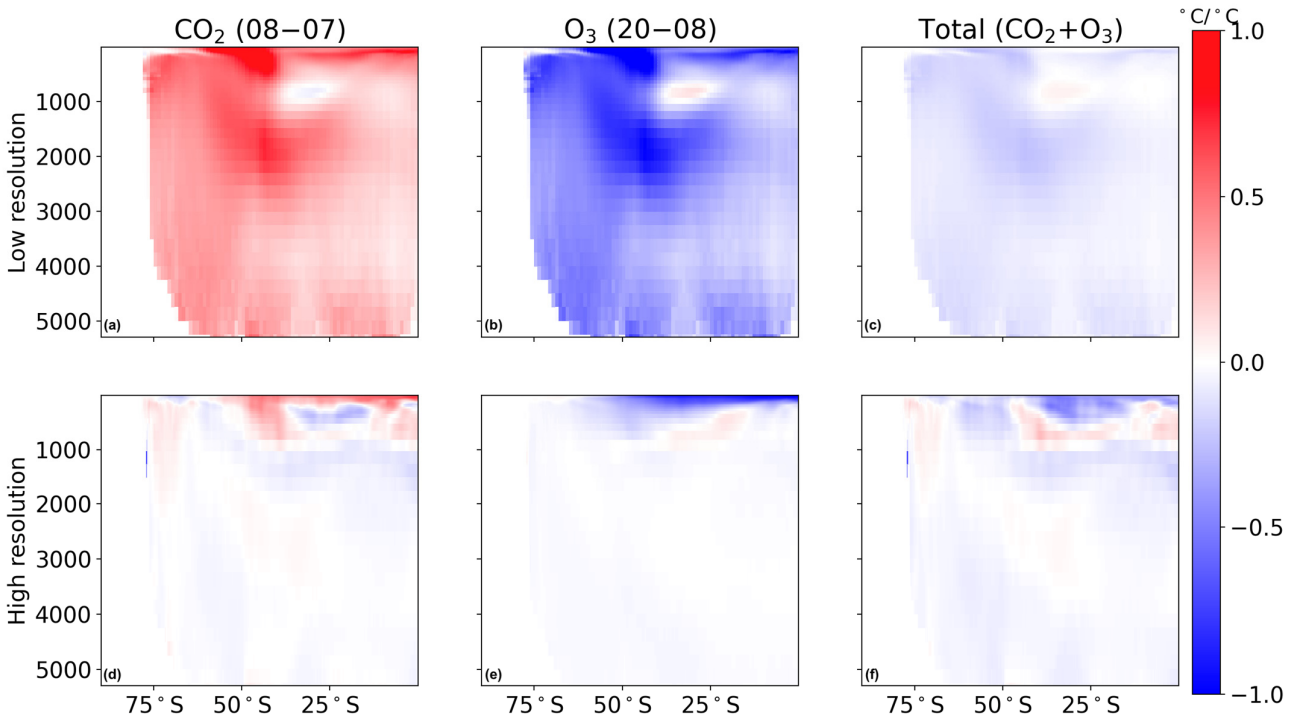

Figure 7. The Southern Hemisphere zonal mean ocean temperature in the eddy-parameterizing simulations (**a**–**c**) and eddy-resolving simulations (**d**–**f**) for the increased CO_2 concentrations (**a**,**d**), past ozone from 1955 (**b**,**e**), and net change (**c**,**f**).The ocean depth in meters is shown on the y-axis, and the latitude is shown on the x-axis. The white, where there are no values, is the bathymetry to the ocean floor from Antarctica at the high latitudes.

3.7. Convective Precipitation

The convective precipitation is analyzed (Figure 8) rather than the total precipitation due to its stronger signal and more localized relationship with SST. The results from the eddy-parameterizing simulations are found to differ greatly from the eddy-resolving simulations. In LRC_{CO_2} (Figure 8a), there is a general increase in convective precipitation but with significant spatial heterogeneity. For example, there is an increase in convective precipitation over the equatorial regions, especially the Pacific, over all of Australia, southern South America, eastern South Africa, and over the western boundary current regions. However, there is a decrease in convective precipitation found over northern and central South America and the rest of Africa. HRC_{CO_2} (Figure 8d) varies significantly from the low-resolution equivalent and shows an increase over eastern and southern Africa, the tropical Indian Ocean, the Pacific Islands, the equatorial Pacific Ocean, and western South America. There is also a decrease seen over parts of Africa, Australia, just south of the equatorial Pacific, eastern South America, and the western boundary currents and their extensions as CO_2 concentrations increase. The difference in the observed average change

between the two is similar in magnitude but opposite in sign, with 0.037 mmday^{-1}/°C and −0.025 mmday^{-1}/°C in LRC_{CO_2} and HRC_{CO_2}.

Once again, a similar but opposite pattern is seen in LRC_{O_3} (Figure 8b) and LRC_{CO_2}. However, the HRC_{O_3} (Figure 8e) convective precipitation pattern looks much different from the LRC_{O_3} simulation, as was seen in the CO_2 simulation. HRC_{O_3} surprisingly resembles the LRC_{CO_2} simulation (Figure 8a), however, especially with the same precipitation pattern found over the Pacific. There is a decrease in convective precipitation seen across all Southern Hemisphere land, with the ozone set to 1955 levels in the high-resolution case. Unlike the CO_2 concentration simulations, the average change in the Southern Hemisphere convective precipitation is the same sign, but the high-resolution magnitude is much smaller than the low-resolution, with a change of −0.045 mmday^{-1}/°C in LRC_{O_3} and −0.010 mmday^{-1}/°C in HRC_{O_3}.

The overall net change seen in LRC_{Total} (Figure 8c) is small, with the average throughout the Southern Hemisphere close to zero, −0.008 mmday^{-1}/°C. However, the pattern is similar to the one seen for past ozone forcing, with the exception of Australia, which shows a total increase in convective precipitation as in the increased CO_2 concentration simulations. On the contrary, the CO_2 forcing dominates everywhere in HRC_{Total} (Figure 8f) except over land, where the ozone forcing is stronger and leads to cooling and an associated decrease in precipitation. Additionally, HRC_{Total} differs from LRC_{Total}, particularly concerning convective precipitation over land. There is a decrease in convective precipitation found in the eddy-resolving simulation compared to an increase found in the eddy-parameterizing simulation. The average change in magnitude increases four times compared to the low-resolution simulation, with a value of −0.035 mmday^{-1}/°C observed. The strong discrepancies observed in convective precipitation across all experiments again highlight the need to use high-resolution models for a chance to accurately model the precipitation variability, which can be detrimental for regions affected by floods and droughts.

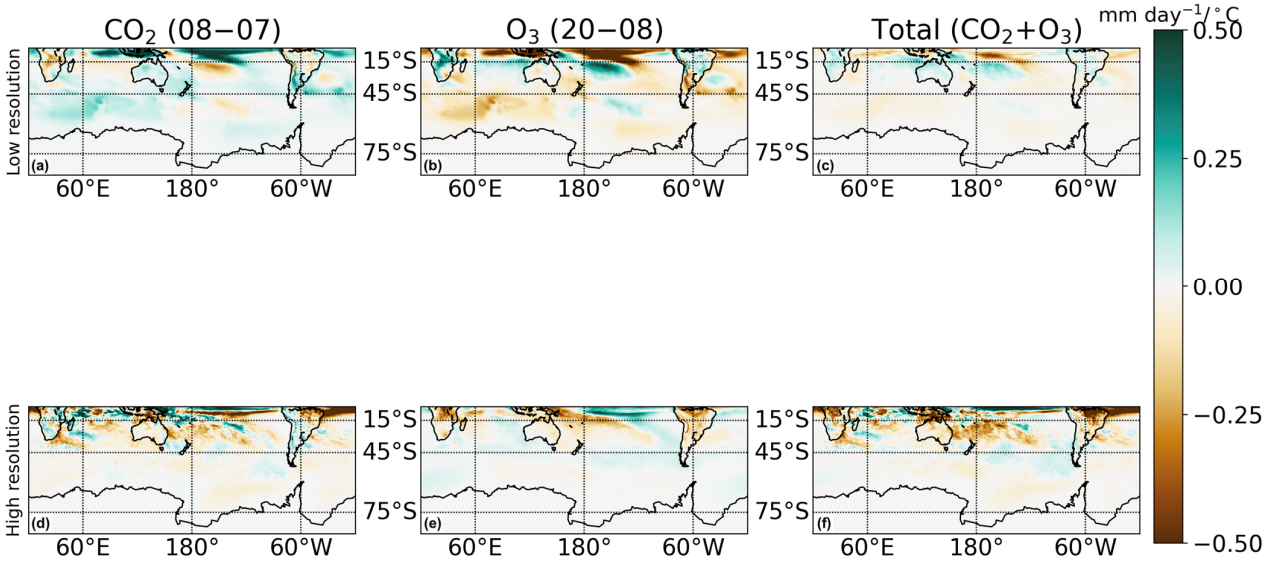

Figure 8. The Southern Hemisphere convective precipitation in the eddy-parameterizing simulations (**a**–**c**) and eddy-resolving simulations (**d**–**f**) for the increased CO_2 concentrations (**a**,**d**), past ozone from 1955 (**b**,**e**), and net change (**c**,**f**).

3.8. Surface Temperature

Lastly, the surface temperature (2 m) is analyzed (Figure 9), and the results do not differ much from the SST results seen previously (Figure 4). In LRC_{CO_2} (Figure 9a), there is strong warming everywhere in the Southern Hemisphere, especially over the Southern Ocean. Like the SST, there is one small region of cooling found in the South Pacific and a region in South America. The high-resolution map does not differ much from the low-

resolution map. HRC_{CO_2} (Figure 9d) has warmed nearly everywhere other than below 60° S, where there is some strong cooling over Antarctica, which is found to be due to the increase in the atmospheric resolution. This cooling at the high latitudes corresponds to the cooling observed at the surface in the zonal mean temperature map (Figure 2d). There is a strong increase in surface temperature over land and in eddy-rich regions, as in the LRC case. Whereas the pattern between the two does not vary much north of the high latitudes, the low-resolution average change is triple the magnitude of the high resolution, with a change of 0.97 °C/°C found in LRC_{CO_2} and 0.30 °C/°C found in HRC_{CO_2}.

LRC_{O_3} (Figure 9b) shows a similar and opposite pattern to LRC_{CO_2}, with cooling everywhere other than the tiny patches seen in the South Pacific and South America that are warming. The most intense cooling is observed over the Southern Ocean. For HRC_{O_3} (Figure 9e), there is cooling everywhere in the Southern Hemisphere, excluding the area around Antarctica, which shows warming. The intense cooling seen over the Southern Ocean does not exist in the eddy-resolving case, as in the SST case. The average change in LRC_{O_3} is −1.14 °C/°C and −0.70 °C/°C in HRC_{O_3}.

The net change in LRC_{Total} (Figure 9c) is weak once again but more closely resembles the ozone forcing aside from Africa and South America, which have increasing surface temperatures and are responding to the increase in CO_2. Australia, Chile, and eastern South Africa have a similar cooling pattern as in the ozone case, likely because these are desert regions and undergo extreme cooling. Finally, the HRC_{Total} (Figure 9f) is dominated by the ozone everywhere other than the eddy-rich regions and below 60° S, which shows that the increase in CO_2 concentrations is more important. Similar to the SSTs, the heat trapped within the eddies is overpowering the cooling seen from the ozone signal and showing a strong net warming change overall. The overall average change is found to be smaller in LRC_{Total} than in HRC_{Total}, with −0.17 °C/°C in LRC_{Total} and −0.41 °C/°C in HRC_{Total}.

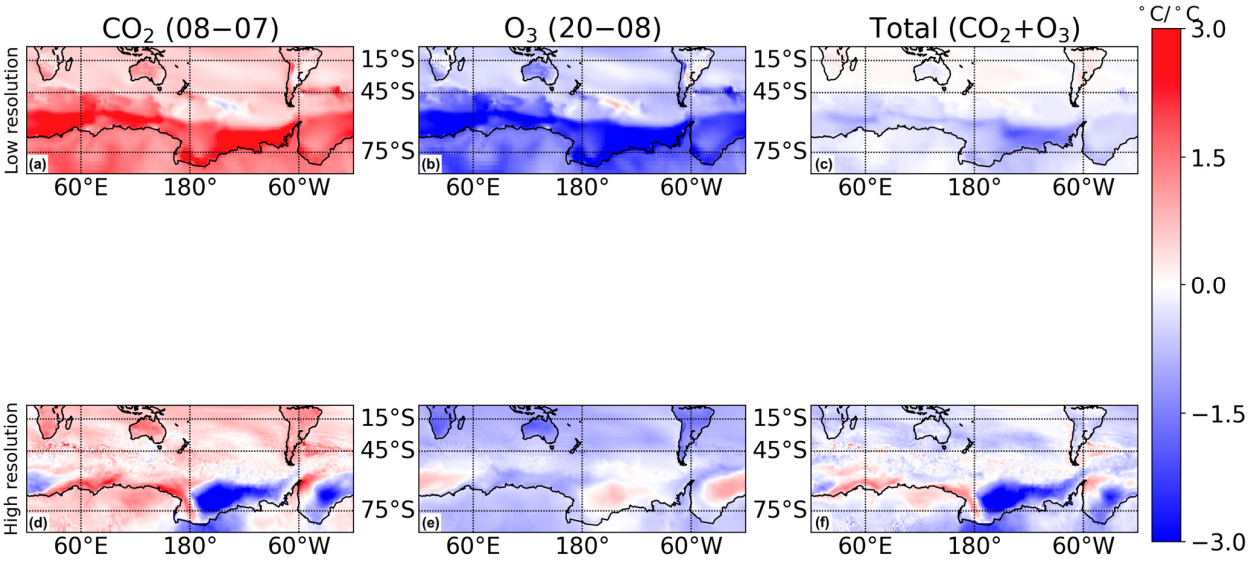

Figure 9. The Southern Hemisphere surface temperature (2 m) in the eddy-parameterizing simulations (**a**–**c**) and eddy-resolving simulations (**d**–**f**) for the increased CO_2 concentrations (**a**,**d**), past ozone from 1955 (**b**,**e**), and net change (**c**,**f**).

4. Discussion

For both the zonal mean atmospheric temperature and the zonal mean zonal wind, the difference between the eddy-parameterizing and eddy-resolving simulations shows a significant difference in the magnitude of change, with more subtle differences in the spatial pattern of the response. For the zonal mean temperature, in the eddy-parameterizing simulations, the 1955 ozone forcing dominates the lower stratosphere at the high latitudes,

with almost no net change seen elsewhere. However, in the eddy-resolving simulations, the ozone forcing is strong throughout the Southern Hemisphere, whereas both the CO_2 and ozone concentrations affect the lower stratosphere at high latitudes. In the low-resolution eddy-parameterizing simulation, the increased CO_2 and 1955 ozone levels are nearly equal and opposite for the zonal mean zonal wind, with no shift of the westerlies observed. In the high-resolution eddy-resolving experiment, the increased CO_2 concentrations dominate the equatorward of 40° S and the ozone forcing poleward of 40° S, with the westerly jet shifting equatorward overall. For the sea surface temperatures in the eddy-parameterized simulations, the increase in CO_2 concentrations and 1955 ozone levels are found to be nearly equal but opposite of each other, with a small overall change observed. In the case of the eddy-resolving simulations, the ozone forcing (cooling) dominates throughout the Southern Hemisphere, apart from eddy-rich regions like the ACC, where the increase in CO_2 response is stronger (warming). However, in the Southern Ocean near Antarctica, there is an overall weaker response in the sea surface temperatures, likely a result of eddy compensation as the mesoscale eddies prevent wind-driven upwelling in the region. In the eddy-parameterizing simulations, the ozone plays a slightly larger role in the sea surface height, eddy kinetic energy, zonal mean ocean temperature, and convective precipitation. For the eddy-resolving simulations, however, the increase in CO_2 concentrations dominates, with the HRC_{Total} spatial maps closely resembling the increased CO_2 concentration experiment (HRC_{CO_2}). For the surface temperature in the eddy-parameterizing simulations, the increase in CO_2 concentration–response (warming) is stronger over Africa and South America. Still, over Australia and the Southern Ocean, the 1955 ozone forcing is more important (cooling). In the eddy-resolving simulation, the ozone is stronger everywhere (cooling), including over land, except in eddy-rich regions and the Southern Ocean near Antarctica. The response of the surface temperature over Australia is unique. In both the eddy-parameterizing and eddy-resolving simulations, Australia is seen to be cooling in response to the 1955 ozone levels. This is in contrast to Africa and South America warming as a result of the increased CO_2 concentrations in the eddy-parameterizing simulations.

The mean change over the entire Southern Hemisphere is calculated to give a quantitative assessment of the changes observed in each simulation to showcase the importance model resolution has on each variable. For the zonal mean atmospheric temperature, the average change in LRC_{Total} is 0.09 °C/°C, nearly zero, whereas the average change in HRC_{Total} is −0.80 °C/°C. The zonal mean zonal wind shows a similar but opposite average change with $-0.26\ ms^{-1}/°C$ in LRC_{Total} and $0.23\ ms^{-1}/°C$ in $HRC_{Total,}$ likely as a result of the increase in the strength of the westerlies from an increase in CO_2 emissions. The average changes in the sea surface temperature and sea surface height are similar to the zonal mean atmospheric temperature. In LRC_{Total}, the changes are almost zero, with a value of −0.07 °C/°C for SST and 0.004 m/°C for SSH. In HRC_{Total}, the changes are −0.24 °C/°C for SST, a change nearly four times that of LRC_{Total}, and −0.027 m/°C for SSH. The eddy kinetic energy average change is similar to what was seen for the zonal mean zonal wind, with the LRC_{Total} and HRC_{Total} being of similar values but opposite signs, $0.55\ cm^2s^{-2}/°C$ and $-0.65\ cm^2s^{-2}/°C$, respectively. There is no difference in the average change for the zonal mean ocean temperature, with −0.09 °C/°C for LRC_{Total} and −0.10 °C/°C for HRC_{Total}. Similar to the zonal mean atmospheric temperature, SST, and SSH, LRC_{Total} for the convective precipitation is nearly zero at $-0.008\ mmday^{-1}/°C$, whereas in HRC_{Total}, it is four times stronger at $-0.035\ mmday^{-1}/°C$. Lastly, the surface temperature shows a significant difference in the overall mean change between the low-resolution and high-resolution simulations, with a change of −0.17 °C/°C for LRC_{Total} and a change of −0.41 °C/°C for HRC_{Total}.

These results show that the model resolution (eddy-parameterizing versus eddy-resolving) proves to be important in how the Southern Hemisphere responds to changes in external forcing (increased CO_2 concentrations versus 1955 ozone levels). The findings outlined above in this study confirm what was shown by previous studies that investigated the importance of model resolution in a changing climate [17,18,29–31]. While this is a

reassuring result, it can be argued that to properly simulate the climate system, higher resolution in the atmospheric and ocean models is needed. With the current model resolution described in this study, neither model accurately resolves the convection in the atmosphere or ocean, as the atmospheric model is in hydrostatic approximation, and the ocean model would need higher resolution, especially at the poles. Perhaps improving the atmospheric model resolution from $1/2^\circ$ to $1/4^\circ$ and the ocean model from $1/10^\circ$ to $1/25^\circ$ would better simulate the climate system in the Southern Hemisphere.

5. Conclusions

This paper, using CCSM4, investigates the role model resolution plays in simulating the Southern Hemisphere climatic response to external forcing from changes in CO_2 and O_3. Low-resolution eddy-parameterizing (1° atmosphere and ocean) and high-resolution eddy-resolving ($1/2^\circ$ atmosphere, $1/10^\circ$ ocean) simulations are analyzed to determine the importance of the mesoscale processes in idealized climate experiments using past CO_2 concentrations and ozone levels. Six experiments were used to study the impact of model resolution on the Southern Hemisphere with increased CO_2 concentrations and past ozone forcing in both the atmosphere and the ocean. These were LRC07 and HRC07 (20th-century climate change forcing, the constant year 2000 ozone levels), LRC08 and HRC08 (the constant year 2000 CO_2 and ozone levels), and LRC20 and HRC20 (the constant year 2000 levels and the constant year 1955 ozone levels).

Before quantitative comparisons can be made across the experiments, the initial results are normalized as the radiative forcing associated with the changes in CO_2 and O_3 is different. The results are normalized by the global mean surface air temperature, with the normalized quantities interpreted as the response per degree of global mean temperature change. This method has been used in many previous studies, as discussed in the Methods section.

To determine the impact the ozone levels and CO_2 concentrations have on the low-resolution and high-resolution simulations, LRC_{CO_2} and HRC_{CO_2}, LRC_{O_3} and HRC_{O_3}, and LRC_{Total} and HRC_{Total} are calculated. From these results, it is determined that overall, in the eddy-parameterizing simulations, the influence of the 1955 ozone levels is found to be more dominant than the increase in CO_2 concentrations. However, in the case of the eddy-resolving simulations, the opposite is found to be true, with the increase in CO_2 concentrations having a larger impact on the Southern Hemisphere climate system than the 1955 ozone levels, especially in eddy-rich regions.

There are a few caveats to note with the conclusion of this study. The first is that this is an idealized study, and the results presented are not to be interpreted as projections or predictions of future climate but rather as an investigation of how extreme changes in the external forcing can lead to different responses in the eddy-parameterizing and eddy-resolving simulations. Additionally, while it has been shown that the ozone forcing is strongly seasonal, with its largest impact observed in austral summer (DJF), all months are considered in the time-averaged mean in this study. This is conducted for both the 20th-century CO_2 and 1955 O_3 levels experiments, so the results are consistent with each other.

The differences observed in the Southern Hemisphere in response to changes in model resolution are significant and emphasize the need for an increase in model resolution going forward, especially in climate prediction studies. Global coupled-climate models in the past were eddy-parameterizing, and this study shows that the results may vary considerably if the models were eddy-resolving. This will be increasingly important as CO_2 concentrations continue to increase and there is a need for more accurate climate forecasts, especially in instances where the associated warming from the CO_2 forced signal overcomes the cooling response associated with the O_3.

Author Contributions: Conceptualization, H.D. and B.P.K.; data curation, H.D. and B.P.K.; formal analysis, H.D.; funding acquisition, B.P.K.; investigation, H.D.; methodology, H.D. and B.P.K.; project administration, B.P.K.; supervision, B.P.K.; writing—original draft preparation, H.D.; writing—review and editing, H.D. and B.P.K. All authors have read and agreed to the published version of the manuscript.

Funding: The authors acknowledge the support from the National Oceanic and Atmospheric Administration (NA18OAR4310293, NA15OAR4320064), the National Science Foundation (OCE1419569, OCE1559151), and the Department of Energy (DE-SC0019433). Ben P. Kirtman is the William R. Middelthon Chair of Earth Sciences and is grateful for the associated support.

Institutional Review Board Statement: Not applicable.

Informed Consent Statement: Not applicable.

Data Availability Statement: The CCSM4 user guide, description, and code can be downloaded at https://www2.cesm.ucar.edu/models/ccsm4.0/ccsm/ (accessed on 14 September 2023). The CCSM4 data used in this study have been uploaded to Zenodo and can be found at https://doi.org/10.5281/zenodo.7838611 (accessed on 14 September 2023). The code used in this study has been uploaded to Zenodo and can be found at https://doi.org/10.5281/zenodo.7812531 (accessed on 14 September 2023).

Conflicts of Interest: The authors declare no conflict of interest.

References

1. Hewitt, H.T.; Roberts, M.J.; Hyder, P.; Graham, T.; Rae, J.; Belcher, S.E.; Bourdallé-Badie, R.; Copsey, D.; Coward, A.; Guiavarch, C.; et al. The impact of resolving the Rossby radius at mid-latitudes in the ocean: Results from a high-resolution version of the Met Office GC2 coupled model. *Geosci. Model Dev.* **2016**, *9*, 3655–3670. [CrossRef]
2. Small, R.D.; de Szoeke, S.P.; Xie, S.P.; O'Neill, L.; Seo, H.; Song, Q.; Cornillon, P.; Spall, M.; Minobe, S. Air–sea interaction over ocean fronts and eddies. *Dyn. Atmos. Ocean.* **2008**, *45*, 274–319. [CrossRef]
3. Small, R.J.; Msadek, R.; Kwon, Y.O.; Booth, J.F.; Zarzycki, C. Atmosphere surface storm track response to resolved ocean mesoscale in two sets of global climate model experiments. *Clim. Dyn.* **2019**, *52*, 2067–2089. [CrossRef]
4. Small, R.J.; Bryan, F.O.; Bishop, S.P.; Larson, S.; Tomas, R.A. What drives upper-ocean temperature variability in coupled climate models and observations? *J. Clim.* **2020**, *33*, 577–596. [CrossRef]
5. Chang, P.; Zhang, S.; Danabasoglu, G.; Yeager, S.G.; Fu, H.; Wang, H.; Castruccio, F.S.; Chen, Y.; Edwards, J.; Fu, D.; et al. An unprecedented set of high-resolution earth system simulations for understanding multiscale interactions in climate variability and change. *J. Adv. Model. Earth Syst.* **2020**, *12*, e2020MS002298. [CrossRef]
6. Bryan, F.O.; Tomas, R.; Dennis, J.M.; Chelton, D.B.; Loeb, N.G.; McClean, J.L. Frontal scale air–sea interaction in high-resolution coupled climate models. *J. Clim.* **2010**, *23*, 6277–6291. [CrossRef]
7. Kelly, K.A.; Small, R.J.; Samelson, R.M.; Qiu, B.; Joyce, T.M.; Kwon, Y.O.; Cronin, M.F. Western boundary currents and frontal air–sea interaction: Gulf Stream and Kuroshio Extension. *J. Clim.* **2010**, *23*, 5644–5667. [CrossRef]
8. Ma, X.; Jing, Z.; Chang, P.; Liu, X.; Montuoro, R.; Small, R.J.; Bryan, F.O.; Greatbatch, R.J.; Brandt, P.; Wu, D.; et al. Western boundary currents regulated by interaction between ocean eddies and the atmosphere. *Nature* **2016**, *535*, 533–537. [CrossRef]
9. Putrasahan, D.A.; Miller, A.J.; Seo, H. Isolating mesoscale coupled ocean–atmosphere interactions in the Kuroshio Extension region. *Dyn. Atmos. Ocean.* **2013**, *63*, 60–78. [CrossRef]
10. Putrasahan, D.A.; Kamenkovich, I.; Le Hénaff, M.; Kirtman, B.P. Importance of ocean mesoscale variability for air-sea interactions in the Gulf of Mexico. *Geophys. Res. Lett.* **2017**, *44*, 6352–6362. [CrossRef]
11. Gould, W.J.; Schmitz Jr, W.J.; Wunsch, C. Preliminary field results for a mid-ocean dynamics experiment (MODE-0). *Deep. Sea Res. Oceanogr. Abstr.* **1974**, *21*, 11. [CrossRef]
12. Mode Group. The mid-ocean dynamics experiment. *Deep Sea Res.* **1978**, *25*, 859–910. [CrossRef]
13. McWilliams, J.C. A review of research on mesoscale ocean currents. *Rev. Geophys.* **1979**, *17*, 1548–1558. [CrossRef]
14. McWilliams, J.C.; Owens, W.B.; Lien Hua, B. An objective analysis of the POLYMODE Local Dynamics Experiment. Part I: General formalism and statistical model selection. *J. Phys. Oceanog.* **1986**, *16*, 483–504. [CrossRef]
15. Polzin, K.L. Mesoscale eddy–internal wave coupling. Part II: Energetics and results from PolyMode. *J. Phys. Oceanog.* **2010**, *40*, 789–801. [CrossRef]
16. Kirtman, B.P.; Bitz, C.; Bryan, F.; Collins, W.; Dennis, J.; Hearn, N.; Kinter, J.L.; Loft, R.; Rousset, C.; Siqueira, L.; et al. Impact of ocean model resolution on CCSM climate simulations. *Clim. Dyn.* **2012**, *39*, 1303–1328. [CrossRef]
17. Bitz, C.M.; Polvani, L.M. Antarctic climate response to stratospheric ozone depletion in a fine resolution ocean climate model. *Geophys. Res. Lett.* **2012**, *39*, L20705. [CrossRef]
18. Bilgen, S.I.; Kirtman, B.P. Impact of ocean model resolution on understanding the delayed warming of the Southern Ocean. *Environ. Res. Lett.* **2020**, *15*, 114012. [CrossRef]
19. McClean, J.L.; Bader, D.C.; Bryan, F.O.; Maltrud, M.E.; Dennis, J.M.; Mirin, A.A.; Jones, P.W.; Kim, Y.Y.; Ivanova, D.P.; Vertenstein, M.; et al. A prototype two-decade fully-coupled fine-resolution CCSM simulation. *Ocean Model.* **2011**, *39*, 10–30. [CrossRef]
20. Putrasahan, D.A.; Beal, L.M.; Kirtman, B.P.; Cheng, Y. A new Eulerian method to estimate "spicy" Agulhas leakage in climate models. *Geophys. Res. Lett.* **2015**, *42*, 4532–4539. [CrossRef]
21. Cheng, Y.; Putrasahan, D.; Beal, L.; Kirtman, B. Quantifying Agulhas leakage in a high-resolution climate model. *J. Clim.* **2016**, *29*, 6881–6892. [CrossRef]

22. Gent, P.R. Effects of Southern Hemisphere wind changes on the meridional overturning circulation in ocean models. *Annu. Rev. Mar. Sci.* **2016**, *8*, 79–94. [CrossRef]
23. Gnanadesikan, A.; Pradal, M.A.; Abernathey, R. Isopycnal mixing by mesoscale eddies significantly impacts oceanic anthropogenic carbon uptake. *Geophys. Res. Lett.* **2015**, *42*, 4249–4255. [CrossRef]
24. Sallée, J.B.; Matear, R.J.; Rintoul, S.R.; Lenton, A. Localized subduction of anthropogenic carbon dioxide in the Southern Hemisphere oceans. *Nat. Geosci.* **2012**, *5*, 579–584. [CrossRef]
25. Wu, L.; Cai, W.; Zhang, L.; Nakamura, H.; Timmermann, A.; Joyce, T.; McPhaden, M.J.; Alexander, M.; Qiu, B.; Visbeck, M.; et al. Enhanced warming over the global subtropical western boundary currents. *Nat. Clim. Chang.* **2012**, *2*, 161–166. [CrossRef]
26. Oliver, E.C.J.; Holbrook, N.J. Extending our understanding of South Pacific gyre "spin-up": Modeling the East Australian Current in a future climate. *J. Geophys. Res. Ocean.* **2014**, *119*, 2788–2805. [CrossRef]
27. Goyal, R.; Sen Gupta, A.; Jucker, M.; England, M.H. Historical and projected changes in the Southern Hemisphere surface westerlies. *Geophys. Res. Lett.* **2021**, *48*, e2020GL090849. [CrossRef]
28. Infanti, J.M.; Kirtman, B.P. A comparison of CCSM4 high-resolution and low-resolution predictions for south Florida and southeast United States drought. *Clim. Dyn.* **2019**, *52*, 6877–6892. [CrossRef]
29. Doddridge, E.W.; Marshall, J.; Song, H.; Campin, J.M.; Kelley, M.; Nazarenko, L. Eddy compensation dampens Southern Ocean sea surface temperature response to westerly wind trends. *Geophys. Res. Lett.* **2019**, *46*, 4365–4377. [CrossRef]
30. Swart, S.; Gille, S.T.; Delille, B.; Josey, S.; Mazloff, M.; Newman, L.; Thompson, A.F.; Thomson, J.; Ward, B.; Du Plessis, M.D.; et al. Constraining Southern Ocean air-sea-ice fluxes through enhanced observations. *Front. Mar. Sci.* **2019**, *6*, 421. [CrossRef]
31. Ivanciu, I.; Matthes, K.; Biastoch, A.; Wahl, S.; Harlaß, J. Twenty-first-century Southern Hemisphere impacts of ozone recovery and climate change from the stratosphere to the ocean. *Weather Clim. Dynam.* **2022**, *3*, 139–171. [CrossRef]
32. Gent, P.R.; Danabasoglu, G.; Donner, L.J.; Holland, M.M.; Hunke, E.C.; Jayne, S.R.; Lawrence, D.M.; Neale, R.B.; Rasch, P.J.; Vertenstein, M.; et al. The community climate system model version 4. *J. Clim.* **2011**, *24*, 4973–4991. [CrossRef]
33. Lamarque, J.F.; Bond, T.C.; Eyring, V.; Granier, C.; Heil, A.; Klimont, Z.; Lee, D.; Liousse, C.; Mieville, A.; Owen, B.; et al. Historical (1850–2000) gridded anthropogenic and biomass burning emissions of reactive gases and aerosols: Methodology and application. *Atmos. Chem. Phys.* **2010**, *10*, 7017–7039. [CrossRef]
34. Lamarque, J.F.; Kyle, G.P.; Meinshausen, M.; Riahi, K.; Smith, S.J.; van Vuuren, D.P.; Conley, A.J.; Vitt, F. Global and regional evolution of short-lived radiatively-active gases and aerosols in the Representative Concentration Pathways. *Clim. Chang.* **2011**, *109*, 191–212. [CrossRef]
35. Lamarque, J.F.; Emmons, L.K.; Hess, P.G.; Kinnison, D.E.; Tilmes, S.; Vitt, F.; Heald, C.; Holland, E.A.; Lauritzen, P.; Neu, J.; et al. CAM-chem: Description and evaluation of interactive atmospheric chemistry in the Community Earth System Model. *Geosci. Model Dev.* **2012**, *5*, 369–411. [CrossRef]
36. Meehl, G.A.; Washington, W.M.; Arblaster, J.M.; Hu, A.; Teng, H.; Tebaldi, C.; Sanderson, B.N.; Lamarque, J.F.; Conley, A.; Strand, W.G.; et al. Climate system response to external forcings and climate change projections in CCSM4. *J. Clim.* **2012**, *25*, 3661–3683. [CrossRef]
37. Eyring, V.; Arblaster, J.M.; Cionni, I.; Sedláček, J.; Perlwitz, J.; Young, P.J.; Bekki, S.; Bergmann, D.; Cameron-Smith, P.; Collins, W.J.; et al. Long-term ozone changes and associated climate impacts in CMIP5 simulations. *J. Geophys. Res. Atmos.* **2013**, *118*, 5029–5060. [CrossRef]
38. Craig, A.P.; Vertenstein, M.; Jacob, R. A new flexible coupler for earth system modeling developed for CCSM4 and CESM1. *Int. J. High Perf. Comp. Appl.* **2012**, *26*, 31–42. [CrossRef]
39. Gent, P.R.; McWilliams, J.C. Isopycnal mixing in ocean circulation models. *J. Phys. Oceanogr.* **1990**, *20*, 150–155. [CrossRef]
40. Ferrari, R.; McWilliams, J.C.; Canuto, V.M.; Dubovikov, M. Parameterization of eddy fluxes near oceanic boundaries. *J. Clim.* **2008**, *21*, 2770–2789. [CrossRef]
41. Fox-Kemper, B.; Ferrari, R.; Hallberg, R.W. Parameterization of mixed layer eddies. Part I: Theory and diagnosis. *J. Phys. Oceanogr.* **2008**, *38*, 1145–1165. [CrossRef]
42. Lin, S.J. A "vertically Lagrangian" finite-volume dynamical core for global models. *Mon. Wea. Rev.* **2004**, *132*, 2293–2307. [CrossRef]
43. Yeager, S.; Danabasoglu, G. Sensitivity of Atlantic meridional overturning circulation variability to parameterized Nordic Sea overflows in CCSM4. *J. Clim.* **2012**, *25*, 2077–2103. [CrossRef]
44. Holland, M.M.; Bitz, C.M. Polar amplification of climate change in coupled models. *Clim. Dyn.* **2003**, *21*, 221–232. [CrossRef]
45. Vecchi, G.A.; Soden, B.J. Global warming and the weakening of the tropical circulation. *J. Clim.* **2007**, *20*, 4316–4340. [CrossRef]
46. Soden, B.J.; Vecchi, G.A. The vertical distribution of cloud feedback in coupled ocean-atmosphere models. *Geophys. Res. Lett.* **2011**, *38*, L12704. [CrossRef]
47. Zhao, C.; Liu, B.; Piao, S.; Wang, X.; Lobell, D.B.; Huang, Y.; Huang, M.; Yao, Y.; Bassu, S.; Ciais, P.; et al. Temperature increase reduces global yields of major crops in four independent estimates. *Proc. Natl. Acad. Sci. USA* **2017**, *114*, 9326–9331. [CrossRef]
48. Lin, L.; Gettelman, A.; Fu, Q.; Xu, Y. Simulated differences in 21st century aridity due to different scenarios of greenhouse gases and aerosols. *Clim. Chang.* **2018**, *146*, 407–422. [CrossRef]
49. Hahn, L.C.; Armour, K.C.; Zelinka, M.D.; Bitz, C.M.; Donohoe, A. Contributions to polar amplification in CMIP5 and CMIP6 models. *Front. Earth Sci.* **2021**, *9*, 710036. [CrossRef]

50. Rantanen, M.; Karpechko, A.Y.; Lipponen, A.; Nordling, K.; Hyvärinen, O.; Ruosteenoja, K.; Vihma, T.; Laaksonen, A. The Arctic has warmed nearly four times faster than the globe since 1979. *Commun. Earth Environ.* **2022**, *3*, 168. [CrossRef]
51. Polvani, L.M.; Previdi, M.; Deser, C. Large cancellation, due to ozone recovery, of future Southern Hemisphere atmospheric circulation trends. *Geophys. Res. Lett.* **2011**, *38*, L04707. [CrossRef]
52. Meredith, M.P.; Naveira Garabato, A.C.; Hogg, A.M.; Farneti, R. Sensitivity of the overturning circulation in the Southern Ocean to decadal changes in wind forcing. *J. Clim.* **2012**, *25*, 99–110. [CrossRef]
53. Morrison, A.K.; Hogg, A.M. On the relationship between Southern Ocean overturning and ACC transport. *J. Phys. Oceanogr.* **2013**, *43*, 140–148. [CrossRef]
54. Marshall, D.P.; Ambaum, M.H.; Maddison, J.R.; Munday, D.R.; Novak, L. Eddy saturation and frictional control of the Antarctic Circumpolar Current. *Geophys. Res. Lett.* **2017**, *44*, 286–292. [CrossRef]